THE AMERICAN SOCIETY OF MECHANICAL ENGINEERS
345 E. 47th St., New York, N.Y. 10017

93-GT-346

ACTIVE STABILIZATION OF ROTATING STALL IN A THREE-STAGE AXIAL COMPRESSOR

Joel M. Haynes, Gavin J. Hendricks, and Alan H. Epstein
Gas Turbine Laboratory
Massachusetts Institute of Technology
Cambridge, MA 02139

ABSTRACT

A three-stage, low speed axial research compressor has been actively stabilized by damping low amplitude circumferentially travelling waves which can grow into rotating stall. Using a circumferential array of hot wire sensors, and an array of high speed individually positioned control vanes as the actuator, the first and second spatial harmonics of the compressor were stabilized down to a characteristic slope of 0.9, yielding an 8% increase in operating flow range. Stabilization of the third spatial harmonic did not alter the stalling flow coefficient. The actuators were also used open loop to determine the forced response behavior of the compressor. A system identification procedure applied to the forced response data then yielded the compressor transfer function. The Moore-Greitzer, 2-D, stability model was modified as suggested by the measurements to include the effect of blade row time lags on the compressor dynamics. This modified Moore-Greitzer model was then used to predict both the open and closed loop dynamic response of the compressor. The model predictions agreed closely with the experimental results. In particular, the model predicted both the mass flow at stall without control and the design parameters needed by, and the range extension realized from, active control.

NOMENCLATURE

A_n	Coefficient of nth spatial harmonic of flow coefficient perturbation
L	Total pressure loss
δL	Perturbation in total pressure loss
n	Spatial harmonic number
P	Static pressure
P_t	Total pressure
δP	Pressure perturbation
r	Compressor annulus mean radius
R	Feedback gain
s_n	$(\alpha_n - i\omega_n)r/U$
t	Time
U	Rotor linear velocity at the mean radius
Z	Complex gain, $Z = R\,e^{i\beta}$
α	Disturbance growth rate
β	Feedback phase angle
ϕ	Flow coefficient, *Axial Velocity/Wheel Speed*
$\delta\phi$	Flow coefficient perturbation
γ	Control vane stagger angle
λ	Inertia parameter for compressor rotors
μ	Inertia parameter for compressor
ϑ	Circumferential coordinate
ρ	Fluid density
τ	Characteristic time
$\bar{\tau}$	Non-dimensional characteristic time
ω	Disturbance frequency
ψ	Total-to-static pressure rise
ψ_t	Torque coefficient, *Torque/(Annulus Area* $\cdot\ \rho U^2 r$*)*

Subscripts

e	Exit
i	Inlet
ideal	Ideal (Euler's Eq.)
IGV	Inlet guide vane
isen	Isentropic
n	Harmonic number
r	Rotor
s	Stator
1	Upstream of IGV's
2	Downstream of control vanes

Superscript

–	Time average

Presented at the International Gas Turbine and Aeroengine Congress and Exposition
Cincinnati, Ohio May 24–27, 1993
This paper has been accepted for publication in the Transactions of the ASME
Discussion of it will be accepted at ASME Headquarters until September 30,1993

TABLE 1
MIT THREE-STAGE AXIAL COMPRESSOR DESIGN PARAMETERS

Tip Diameter (mm.)	610.00
Hub-to-Tip Ratio	0.88
Design Average Reaction	0.75
Design Flow Coefficient	0.59
Pressure Rise Coefficient (@design)	2.03
Efficiency (@design)	84.3%
Stalling Flow Coefficient	0.460

	No. of Blades	Chord (mm.)	Camber (degrees)	Stagger (degrees)	Tip Clearance* (mm)	Leading Edge Blade Angle* (degrees)	Trailing Edge Blade Angle* (degrees)
Inlet Guide Vanes	125	20.1	11.0	8.1		0	10.0
IGV to CV Gap		6.0					
Control Vanes	12	81.2	0.0	8.1		8.1	8.1
CV to R1 Gap		13.0					
Rotor 1	54	45.2	17.0	42.8	0.97	50.0	41.0
R1 to S1 Gap		20.0					
Stator 1	85	31.4	27.0	11.0	0.81	54.5	36.5
S1 to R2 Gap		20.0					
Rotor 2	55	44.8	18.0	43.5	0.94	58.0	38.0
R2 to S2 Gap		20.0					
Stator 2	88	31.3	25.0	12.0	0.94	18.0	-1.0
S2 to R3 Gap		20.0					
Rotor 3	49	50.7	20.0	44.6	0.89	27.5	2.5
R3 to S3 Gap		18.0					
Stator 3	90	31.4	53.0	5.5	0.86	36.5	-17.0

*Measured by Gamache CV = Control Vane IGV = Inlet Guide Vane

INTRODUCTION

Axial flow compressors suffer from inherent hydrodynamic instabilities known as surge and rotating stall. Surge is a one-dimensional mass flow disturbance involving the entire compression system, while rotating stall has a two- or three-dimensional structure rotating about and local to the compressor blading. Both are large amplitude disturbances, disrupting compressor operation and imposing large structural loads, and so are unacceptable in routine compressor operation.

A useful theoretical model of compressor hydrodynamic stability started with Emmons et al. (1955) and has evolved through Moore and Greitzer (1986). In this analysis, surge and rotating stall are simply the mature form of the natural oscillatory modes of the compression system. Surge is the lowest (zero) order mode and rotating stall is the higher order modes. This model predicts that these hydrodynamic disturbances start at very small amplitude (during which time the modes may be considered as linear and decoupled) but quickly grow into their large amplitude form, surge and rotating stall (which exhibit nonlinear behavior and whose dynamics are coupled). Thus, the stability of the compressor is equivalent to the stability of these small amplitude waves which exist prior to stall. Garnier et al. (1991), McDougal et al. (1990), and Etchevers (1992) presented experimental data showing the existence of these low amplitude waves and their evolution into stall in several axial compressors. More recently, Paduano and Gysling (1992) have shown that the details of the time evolution of the disturbances, especially the wave form, is quite sensitive to the shape of the compressor pressure rise versus mass flow characteristic.

Epstein, Ffowcs Williams, and Greitzer (1989) first suggested that surge and rotating stall could be prevented by using active feedback control to damp the hydrodynamic disturbances while they are still at small amplitude. Aside from reducing the control authority required, control of the fluid disturbances while they still are at very low amplitude permits incipient surge and rotating stall to be treated and controlled separately (since their behavior will be linear and decoupled). Active suppression of surge was subsequently demonstrated experimentally on centrifugal compressors by Ffowcs Williams and Huang (1989) and Pinsley et al. (1991), and on an axial compressor by Day (1991). Paduano et al. (1991) demonstrated active suppression of rotating stall in a single-stage low speed compressor. By damping the small amplitude travelling waves rotating about the annulus prior to stall, they increased the stable flow range of the compressor by 25%.

The data of Paduano et al. provides strong experimental evidence that at least the qualitative structure of the hydrodynamic stability theory is appropriate for this type of compressor and that, indeed, rotating stall can evolve from small amplitude travelling waves since damping these waves prevents the formation of rotating stall. In those experiments, the travelling waves were decomposed into separate spatial harmonics with each harmonic controlled individually. This showed that the linear and decoupled behavior predicted by the theory did indeed occur. The theory, however, predicted that all spatial harmonics go unstable at the same mass flow, while the experiment showed that the lower the harmonic, the higher the mass flow at instability. This behavior has an important implication for active control since it means that all spatial harmonics need not be simultaneously controlled in order to

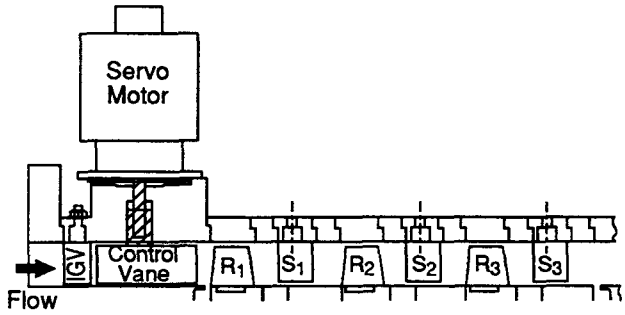

Fig. 1: Three-stage compressor arrangement with individually actuated high speed control vanes.

realize an increase in compressor operating range, greatly simplifying the physical realization of such a control system.

In the work presented herein, we extend the experimental single-stage work of Paduano by applying the same active control techniques to a three-stage, low speed research compressor. Both open loop forced response and closed loop actively stabilized data are presented. We also extend the two-dimensional, incompressible hydrodynamic stability theory of Moore and Greitzer to include non-ideal effects such as time lags associated with the development of viscous losses and deviations. These modifications have the effect of separating in mass flow the inception of the instabilities of individual spatial harmonics as observed by Paduano. We then show that this theory does an excellent job in quantitatively predicting both the open and closed loop dynamic behavior of the three-stage compressor. This includes predicting the natural stall point (inception of rotating stall without control) and predicting both the controller parameters required and the improvement in mass flow range gained from active control. Finally, we make some comments on the utility of an actively stabilized machine for exploration of compressor dynamics.

Experimental Apparatus

A 0.6 meter diameter, three-stage low speed axial research compressor was adapted for use as a test article in these experiments. Work in this rig was previously reported by Gamache (1990), Lavrich (1988), and Garnier et al. (1991). The blading details are given in Table 1. The control scheme adopted was that used by Paduano et al. in which the travelling waves of axial velocity are detected by a circumferential array of hot wires just upstream of the compressor and individually actuated vanes upstream of the rotor are used to generate the rotating disturbance structure required for control. The test compressor was appropriately modified by moving the inlet guide vanes (IGV's) sufficiently far upstream so that control vanes could be placed between the IGV's and the first rotor. In this arrangement, the inlet guide vanes produce the mean swirl while the unchambered control vanes provide the time and circumferential variations

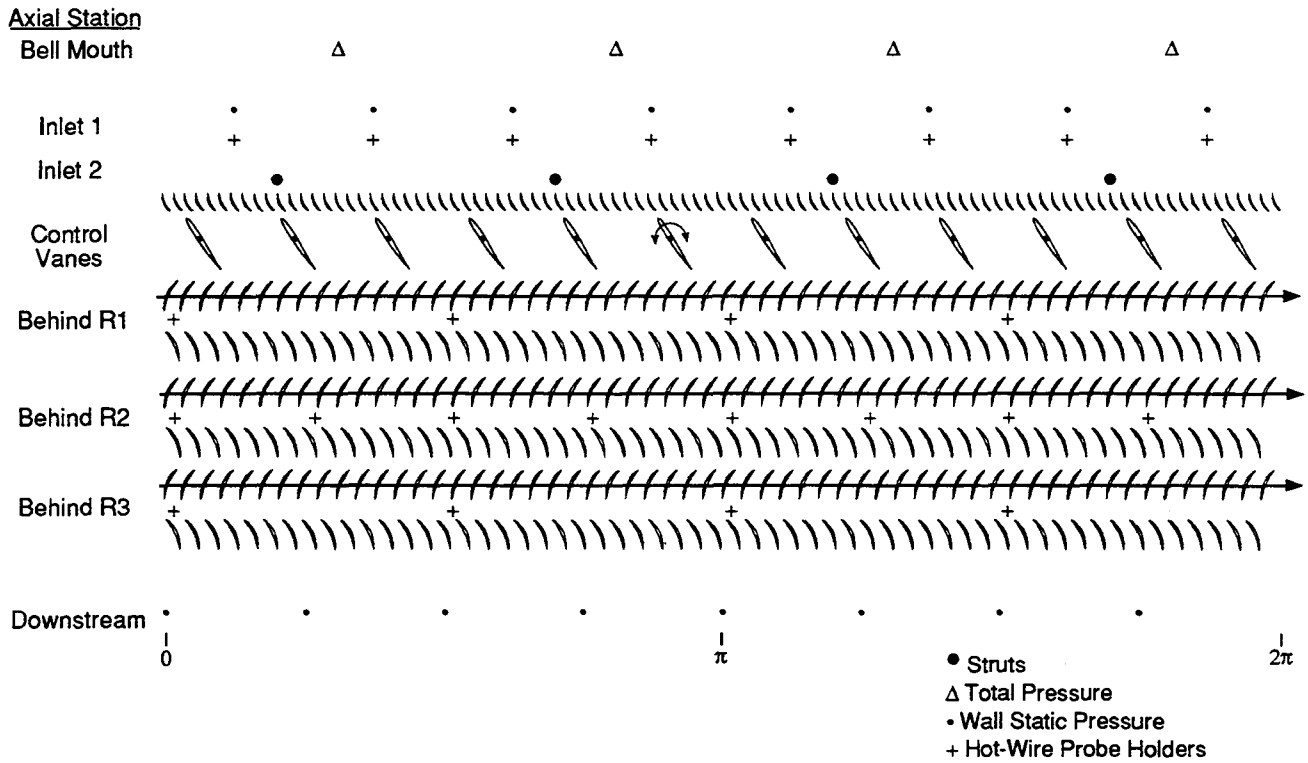

Fig. 2: Layout of compressor blading and instrumentation.

needed to stabilize the compressor. Each of the twelve control vane assemblies consisted of NACA 65-0009 cast epoxy airfoils, cantilevered from a hollow core, high torque to inertia DC servo motor (Fig. 1). Instrumentation included circumferential hot wire, total pressure, and static pressure arrays mounted throughout the compressor (Fig. 2). Additional measurements consisted of rotor speed and torque, average compressor mass flow (from a venturi), and rig housekeeping. The net measurement precision of the flow coefficient (ϕ), the pressure rise coefficient (ψ), the torque coefficient (ψ_t), and the rotor speed were all ±0.3% or better. Control vane angles were measured to ±0.05°. On the stable portion of the compressor characteristic near the point of instability, the signal-to-noise ratios of the first three spatial harmonics were 46 dB, 29 dB, and 23 dB respectively.

The control system hardware is illustrated in Fig. 3. The signals from the eight hot wire anemometers mounted about the compressor circumference are filtered by four-pole Bessel filters set at 1000 Hz, which is 25 times the shaft frequency, ω_s. The signals are then digitized by a 16-bit A/D system in an 80486 computer, which implements the control laws and outputs the commanded control vane positions to individual vane position control systems. These consist of closed loop, PID position servos, one for each channel, feeding 350 watt servo amplifiers which drive the DC servo motors. Optical encoders mounted on each motor provide a vane position signal to the position servos. The vane servo loops operated at 50 ω_s (2000 Hz), while the entire control loop in the computer was operated at 12.5 ω_s (500 Hz). The control vane system dynamic response was determined by driving the vane array with a pseudo-random binary signal with a minimum frequency of 2.5 ω_s (100 Hz), while the compressor was operated near its stall point. These measurements showed that the transfer function of the flow actuation system could be modelled quite closely by two second order systems in series with a natural frequency of 170 Hz and a damping ratio of 0.35. This yields a frequency response flat to ±3 dB up to 3 ω_s (120 Hz). The first spatial harmonic of rotating stall is approximately 0.3 ω_s (12.5 Hz) in this compressor.

The rotating stall control algorithms were similar to those used by Paduano. At each time step, the anemometer data is digitized and linearized into axial velocity; a discrete spatial Fourier transform is then used to decompose the eight velocity measurements into spatial harmonics (only modes 1, 2, and 3 were examined here); a separate control law is then implemented on each spatial harmonic; and then an inverse discrete Fourier transform on the spatial harmonics is taken to yield individual blade position commands to each of the 12 control vane position control systems.

A simple proportional control law was implemented in these experiments. For each spatial harmonic n, the change in control vane stagger angle, γ, is proportional to the measured change in axial velocity, V.

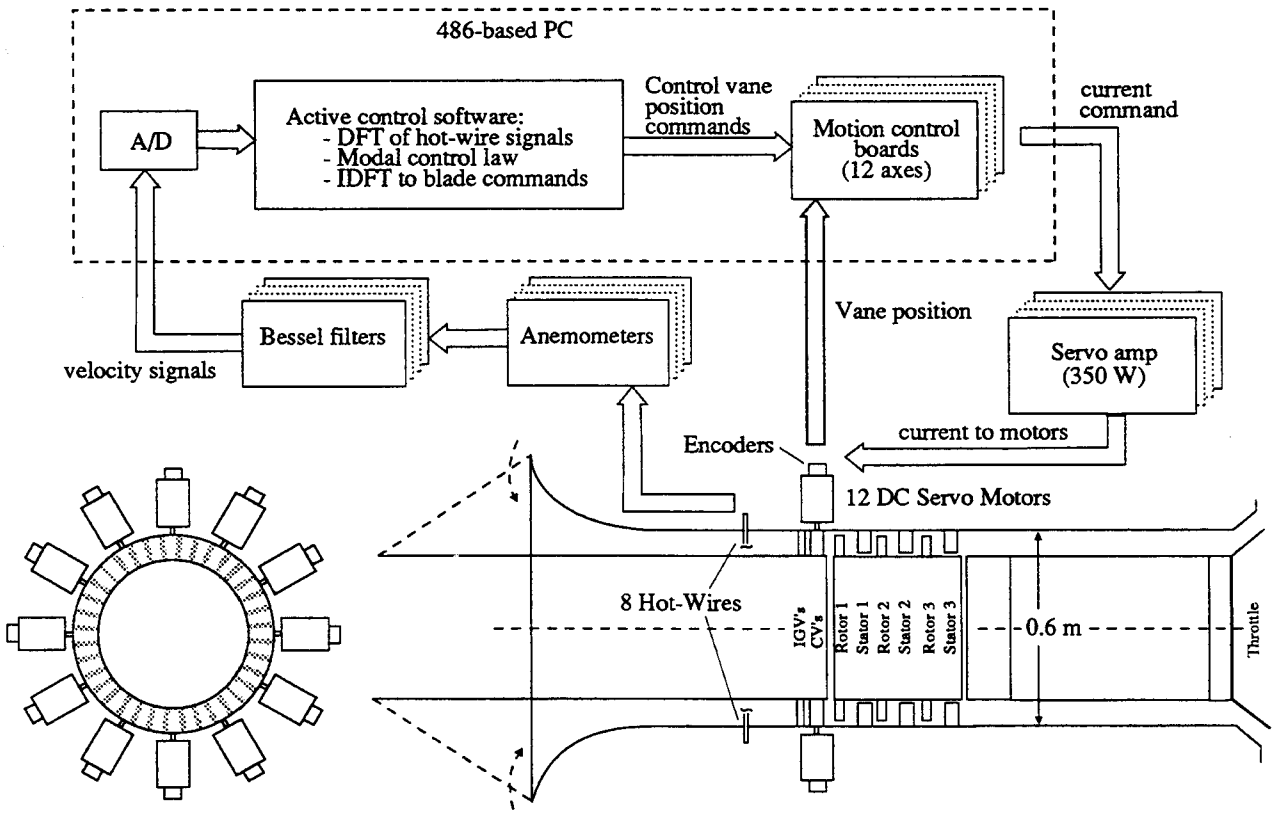

Fig. 3: Closed-loop control feedback path.

$$|\delta\gamma_{vane}|_n = Z_n V_n \quad (1)$$

where Z_n is the complex constant of proportionality

$$Z_n \equiv R_n e^{i\beta_n} \quad (2)$$

R_n represents the gain of the controller, while β_n is the phase angle between the measured velocity perturbation and commanded stagger angle change for each harmonic. With this harmonic by harmonic control scheme, β_n is a spatial lead which can account for both lags in the control system and the dynamics of the compressor. The total change in vane stagger angle is then simply the sum of the deflections calculated for the individual harmonics being studied (1, 2, or 3 in this case). Paduano established the optimum gain and phase for each harmonic empirically. Here, as will be shown later, theory can be used to calculate the optimum feedback gain and phase with results closely matching those found experimentally.

Steady State Compressor Performance

In addition to the active stabilization experiments, steady state measurements were taken both to assess the compressor operating characteristics and to establish the aerodynamic parameters needed as input to the analytical modeling and control law design. These included measurements of the speedline shape, the torque efficiency, and the influence of control vane stagger angle (γ) on the non-dimensional pressure rise coefficient (ψ). Specifically, the $\partial\psi/\partial\gamma$ values required by the theory were derived from measurements of the steady state influence of vane stagger on compressor pressure rise, as illustrated in Fig. 4. The resultant values of $\partial\psi/\partial\gamma$ and $\partial\psi/\partial\phi$ are shown in Fig. 5. Data in the normally unstable low flow area were taken while the compressor was stabilized with feedback control.

Compressor Performance With Active Stabilization

Active feedback stabilization of the first two spatial harmonics was implemented as described above. The results using the optimum feedback gain and phase found are illustrated on the speedline in Fig. 6. Control of the first harmonic yields a range increase of 3%, while control of the first and second harmonics together increase that to 8%. At this point, the speedline slope is 0.9. The compressor torque efficiency continues to decrease smoothly in the actively stabilized region.

It is useful to examine the time history of the transient into stall as an aid in understanding the instability evolution process. The time history of the axial velocity measured by the eight sensors about the compressor circumference is shown in Fig. 7 for the unstabilized compressor. Here, the smooth growth of the first spatial harmonic wave is quite apparent for the 15 rotor revolutions illustrated before stall (it is highlighted by the parallel dotted lines in the figure). When the first spatial harmonic is actively suppressed (Fig. 8), the stall inception process is different

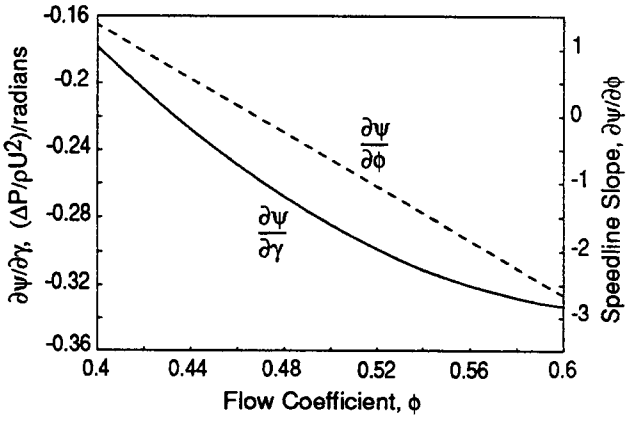

Fig. 5: Variation of speedline slope ($\partial\psi/\partial\phi$) and control vane angle pressure rise influence ($\partial\psi/\partial\gamma$) measured for the three-stage compressor.

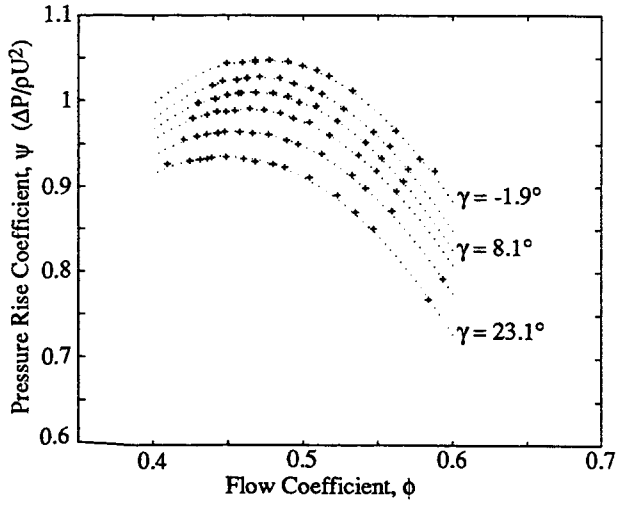

Fig. 4: The influence of uniform control vane stagger angle (γ) on the compressor characteristic at 5° intervals of γ.

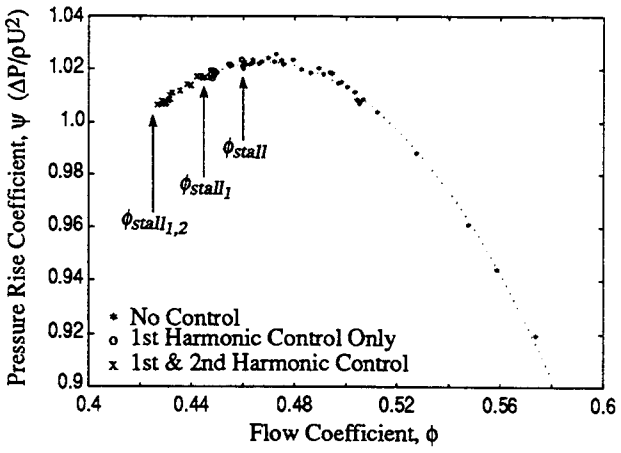

Fig. 6: Active stabilization of the first and second spatial harmonics decreases stalling mass flow by 8%.

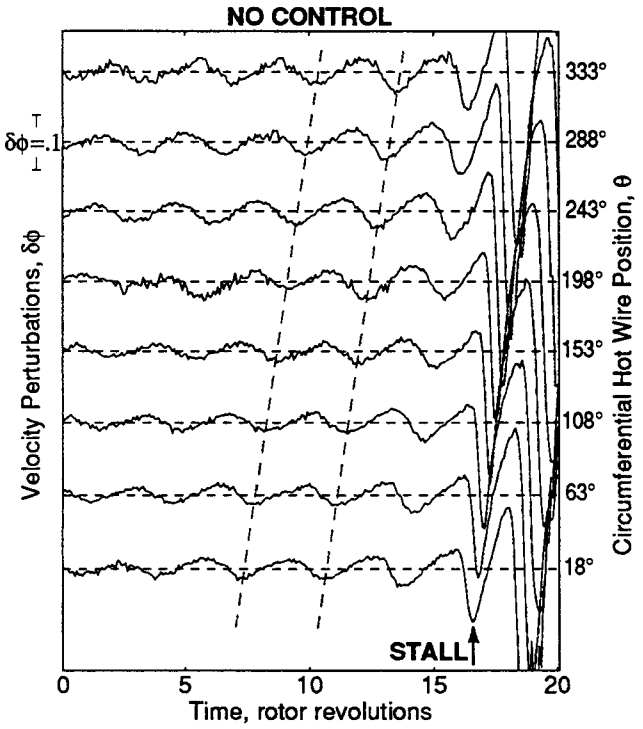

Fig. 7: Stall inception flow field around compressor annulus at midspan, measured upstream of the IGV's when $\bar{\phi}$ = 0.46, with no control.

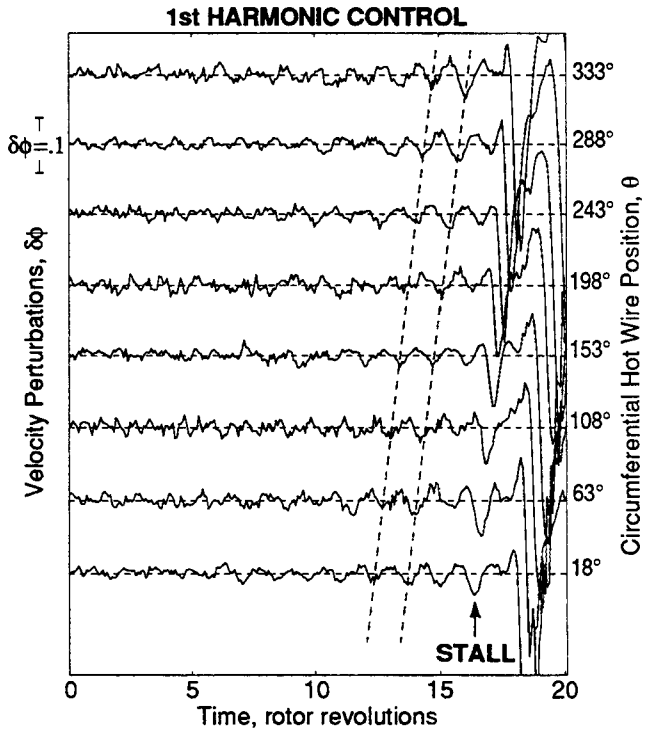

Fig. 8: Stall inception flow field around compressor annulus at midspan during first harmonic control, measured upstream of the IGV's when $\bar{\phi}$ = 0.45.

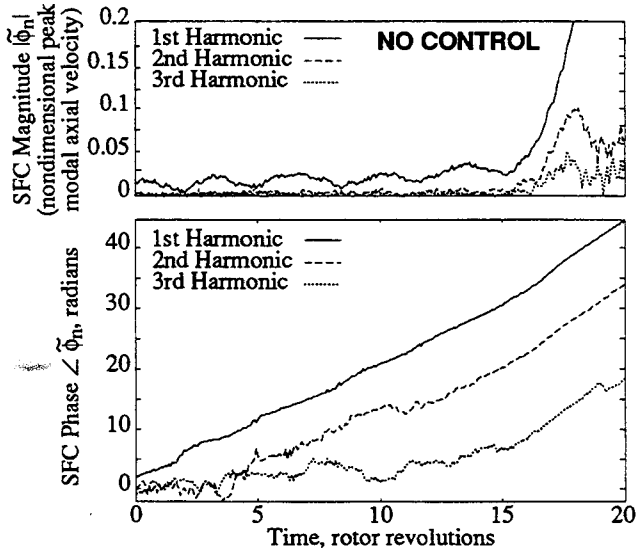

Fig. 9: Magnitude and phases of the first three spatial Fourier coefficients (SFC) calculated from the stall inception flow field at midspan (calculated from the data of Fig. 7).

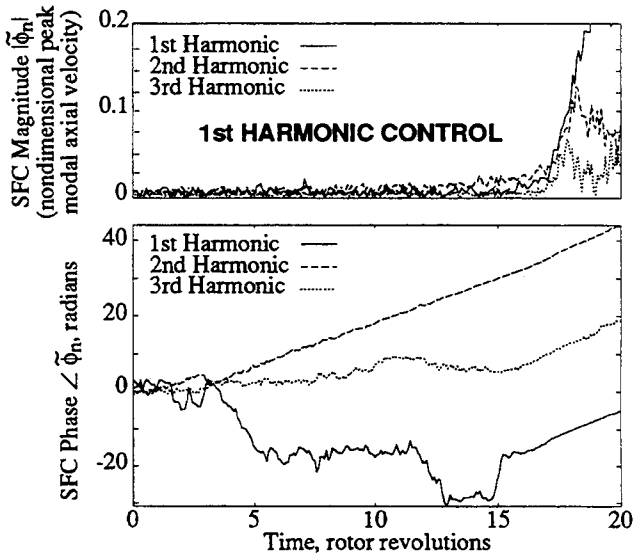

Fig. 10: Magnitude and phases of the first three spatial Fourier coefficients calculated from the stall inception flow field at midspan during first harmonic control (calculated from the data of Fig. 8).

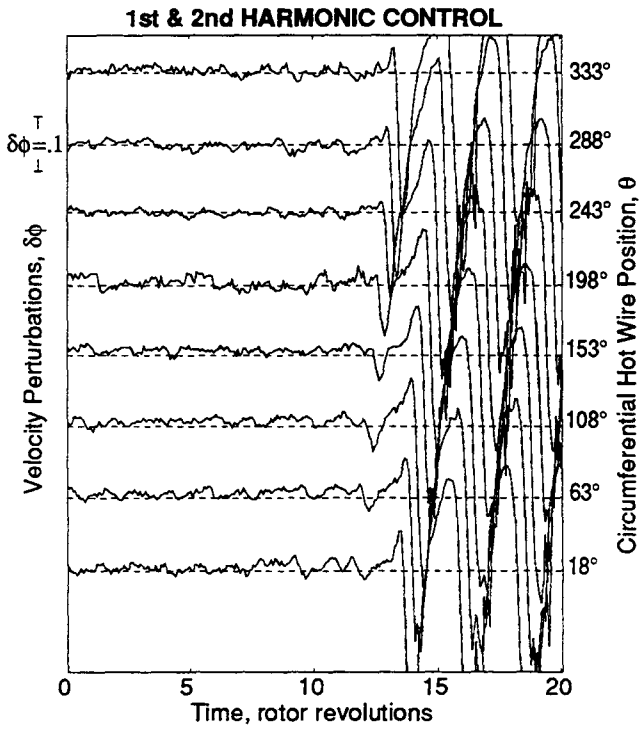

Fig. 11: Stall inception flow field around compressor annulus during optimal first and second harmonic control, measured upstream of the IGV's when $\bar{\phi} = 0.43$.

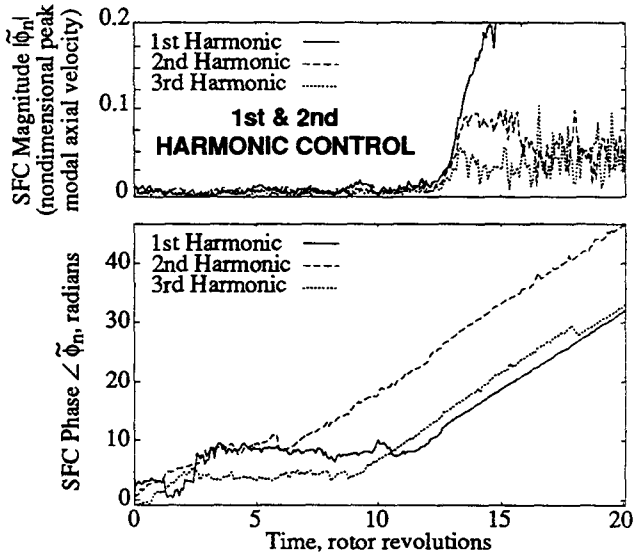

Fig. 12: Magnitude and phases of the first three spatial Fourier coeffients calculated from the stall inception flow field at midspan during optimal first and second harmonic control (calculated from the data of Fig. 11).

in that it occurs at a lower mass flow and that the low amplitude waves growing prior to stall have one half the wavelength, as can be readily seen by comparing Figs. 7 and 8. It is the second spatial harmonic which goes unstable now and triggers the rotating stall when the first harmonic is stabilized.

A useful tool for examining the wave growth is a discrete spatial Fourier transform of the axial velocities measured about the compressor annulus at each instant in time. This yields a complex Fourier coefficient for each spatial harmonic, the magnitude of which represents the instantaneous strength of that spatial wave, and the phase of which is a measure of the instantaneous angular position of the wave. Thus, a straight line phase history indicates that the wave is travelling at constant angular velocity. This behavior can be seen in Fig. 9, which presents the spatial Fourier coefficients calculated from the unstabilized data of Fig. 7. The first harmonic position does change at a constant rate for some 15 revolutions before stall. (Note that the compressor is unwrapped here so that 2π radians represents one revolution of the wave, 4π radians two revolutions, and so on.) Examination of the magnitudes of the first three spatial harmonics in Fig. 9 shows that the first is the strongest and that it grows to large amplitude before the second and third do. This uncontrolled compressor has a single lobed stall (primarily first harmonic) at this mass flow. When the first harmonic is actively stabilized, however, the Fourier coefficient of the second harmonic is strongest prior to stall (Fig. 10). Once stall starts, though, the first harmonic quickly dominates. Indeed, examination of the time history in Fig. 8 shows that once the fully developed rotating stall is established, it is a single lobed stall.

A time history of the compressor under first and second harmonic control is shown in Fig. 11 and the corresponding spatial Fourier coefficients in Fig. 12. Here, the instability appears to grow from both the first and second harmonic, with the third harmonic weaker. Again, the fully developed stall is primarily single lobed. Although the third harmonic does not appear to play a dominant role in Fig. 12, simultaneous stabilization of the first three harmonics was implemented with results shown in Figs. 13 and 14. No increase in stable flow range is achieved over control of only the first and second harmonics. The relative roles played by the three spatial harmonics is not clear from the data in Fig. 14, although the first harmonic does appear to grow first.

We have now presented experimental data showing that a low speed multistage axial compressor can be actively stabilized and illuminating the stall inception processes in this machine. We will now use this data as an aid in refining an analytical model of instability inception and show both how this model can quantitatively predict many details of stall inception and how the model can be used to design an active control system.

MODELING

The two-dimensional, incompressible theory formulated by Moore and Greitzer to describe rotating stall implies that, at the inception of the instability, small amplitude travelling waves develop in the compressor annulus, grow in magnitude, and eventually develop into rotating stall cells. In this analysis of instability inception, an arbitrary axial velocity disturbance is decomposed into its Fourier spatial harmonics which can then be

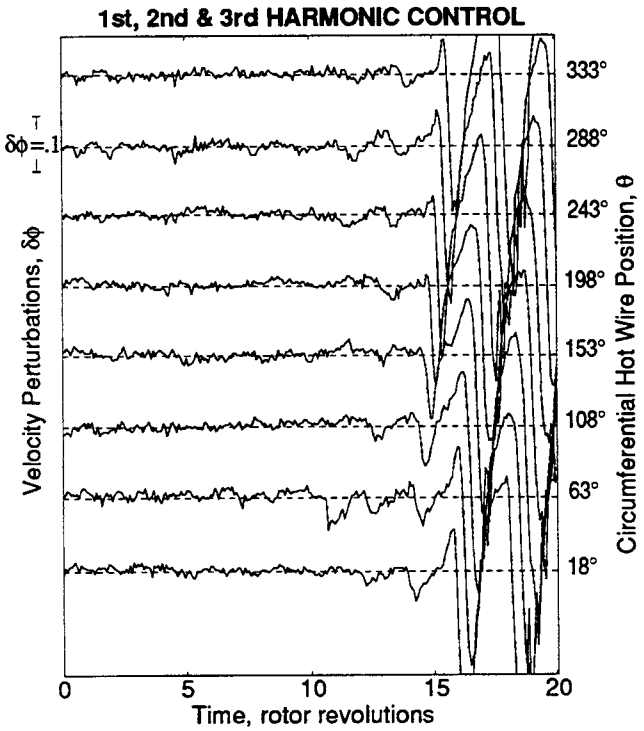

Fig. 13: Stall inception flow field around compressor annulus during optimal first, second and third harmonic control, measured upstream of the IGV's when $\bar{\phi} = 0.43$.

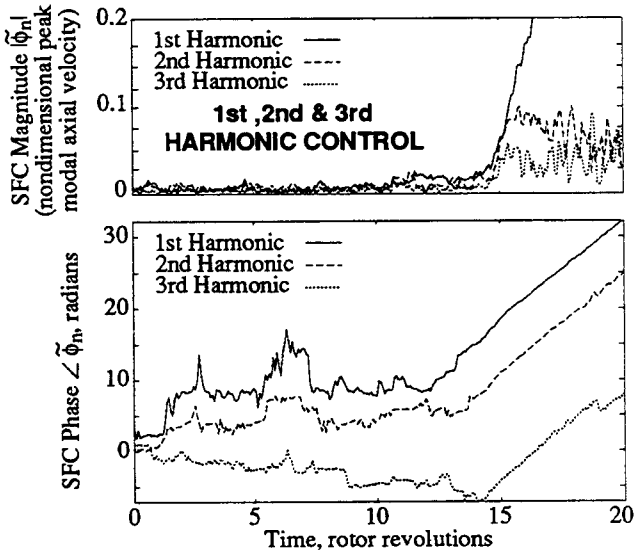

Fig. 14: Magnitude and phases of the first three spatial Fourier coeffients calculated from the stall inception flow field at midspan during optimal first, second and third harmonic control (calculated from the data of Fig. 13).

analyzed independently, since the equations describing the evolution of the instability are linear. If the compressor is assumed to operate in a quasi-steady manner, i.e. pressure rise is a function of flow coefficient only, this model predicts that all the spatial harmonics of the flow coefficient perturbation become unstable at the operating point where the total-to-static pressure rise characteristic (ψ vs. ϕ) becomes positively sloped. Disturbances are damped where the characteristic is negatively sloped, and amplified where the characteristic is positively sloped, with the growth or decay rate of the perturbation being determined by the magnitude of the slope.

Contrary to the assumptions of the above model, airfoils do not respond instantaneously to changes of incidence, and it has been observed in experiments (Nagano et al., 1971; Mazzawy, 1977) that the pressure rise across a compressor does not respond instantaneously to variations in flow coefficient. As will be shown, this finite response time of the compressor pressure rise has a stabilizing effect on flow perturbations, stabilizing higher harmonics to a greater extent than lower ones. When the quasi-steady assumption in the model is relaxed, and allowance is made for finite blade-passage flow response times, the spatial harmonics become unstable sequentially, with higher harmonics becoming unstable at larger positive slopes of the compressor total-to-static pressure-rise characteristic (i.e. lower flow coefficients). This is the behavior observed in the experiments on both the three-stage compressor being discussed, and previous experiments on a single-stage compressor (Paduano, 1991; Paduano et al., 1991).

In the following sections, the model is extended to include the finite response time and the results are compared to experimental data.

ACCOUNTING FOR BLADE ROW PRESSURE LOSSES, DEVIATION AND BLOCKAGE

Current 2-D models of compressor stability like that of Moore and Greitzer are quite simplified. In these analyses, the compressor is described only in terms of the slope of its pressure rise–mass flow characteristic and the inertia of the fluid in the blade rows. The effects of physical phenomena important to the compressor designer such as stagnation pressure losses, deviations, blockage, and characteristic airfoil response times had not been treated explicitly in these models since little data was available to evaluate their influence on compressor stability. The actively stabilized compressor rig is a tool with which such data may be acquired so that we can now evaluate the relative importance of these phenomena and modify the analysis accordingly.

To start, we will quantify the effects of deviation, blockage, and airfoil unsteady response on the measured compressor pressure rise. In an ideal compressor with none of the above, the ideal pressure rise (ψ_{ideal}) can be calculated with the Euler equation and decreases monotonically with increasing flow coefficient, as can be seen in Fig. 15. The difference between this ideal pressure rise and the actual measured one (ψ) is due to the combined effects of lack of flow turning (due to both deviation as specified in Carter's rule and blockage which is the result of viscous effects) and total pressure losses (viscous dissipation in all compressors plus shock losses in transonic machines). To

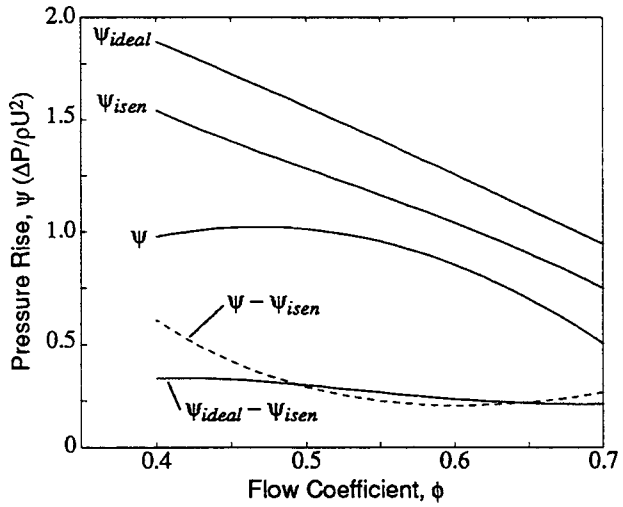

Fig. 15: The difference between the ideal pressure rise (ψ_{ideal}) and the isentropic pressure rise (ψ_{isen}) is due to deviation, while the difference between the measured pressure rise (ψ) and ψ_{isen} is due to total pressure losses.

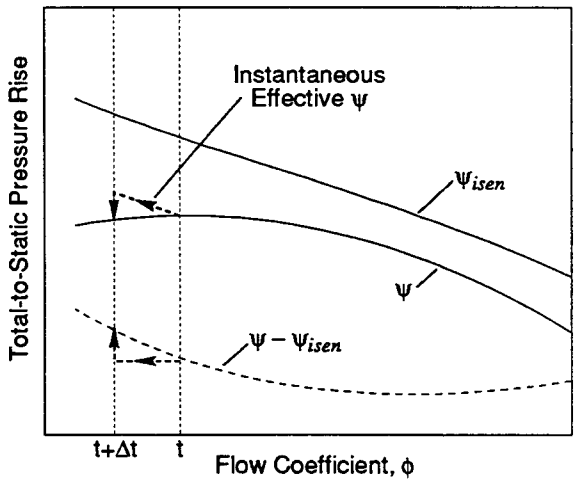

Fig. 16: Compressor time lags temporarily decrease the effective slope of the compressor characteristic during a transient, as illustrated starting at time, *t*.

separate the two effects, consider the case when the compressor is operating isentropically so that all of the shaft work goes into stagnation pressure rise. This isentropic stagnation pressure rise (ψ_{isen}) can be calculated from the measured shaft torque, ψ_t, as:

$$\psi_{isen} = \left[\frac{\psi_t}{\phi} - \frac{\phi^2}{2\cos^2 \varepsilon_e} \right] \tag{3}$$

where ε_e is the exit flow angle from the last stator. The isentropic pressure rise characteristic of this compressor is shown in Fig. 15. The loss in pressure rise represented by the difference between the ideal (ψ_{ideal}) and the isentropic (ψ_{isen}) pressure rises must be due to lack of turning (i.e. deviation and blockage). While the loss in pressure rise represented by the difference between the isentropic rise (ψ_{isen}) and the measured rise (ψ) must be due to total pressure losses (viscous dissipation). These are illustrated in Fig. 15.

The important information in Fig. 15 is that, for the three-stage compressor considered here, the total pressure losses due to dissipation, (ψ - ψ_{isen}), increase significantly with reduction of flow coefficient over the range of interest (to the left of the peak of the measured characteristic). On the other hand, the loss due to the deviation (ψ_{ideal} - ψ_{isen}), is relatively flat over this range. Thus, we would expect the influence of dissipation on compressor stability to be considerably larger than that of deviation. Both were modelled and, in fact, the influence of deviations proved negligible so that in the following sections we will only discuss the role of dissipation. We have not studied the generality of this observation to all compressors but have merely exploited it to simplify the modeling (more details may be found in Haynes (1992)). We note, however, that Longley and Hynes (1989) reported deviation to be more important in their compressor than the one studied here.

MODELING COMPRESSOR TRANSIENT BEHAVIOR

Dissipation influences compressor stability because of the time lags the viscous flow introduces. An instantaneous change in mass flow (axial velocity) abruptly changes the compressor blading angle of attack. The flow over the blades does not change instantaneously, however; rather it evolves to the new steady state over a time period on the order of the bulk convection time through the blade rows. Emmons et al. (1955) suggested modeling the evolution of losses as a first order lag. For the step reduction in ϕ, the change in stagnation pressure loss δL is then given by:

$$\delta L_{transient} = \delta L_{quasi-steady} \left(1 - e^{-t/\tau}\right) \tag{4}$$

where τ is the characteristic time.

Since the instantaneous stagnation pressure losses reflect the time lags associated with the flow within the compressor blade passages, the compressor pressure rise must as well. To illustrate this point, consider an instantaneous reduction in flow coefficient when the compressor is operating on a positive sloped portion of the characteristic (Fig. 16). Immediately after the reduction in flow coefficient, the stagnation pressure loss is at its initial value, so that the actual pressure rise follows as a curve parallel to the isentropic pressure rise (ψ_{isen}), as shown in Fig. 16. The transient slope is thus less than the steady-state one, so that the compressor is more stable than it is in steady state at the same mass flow. In the operating range where the compressor characteristic slope is positive (and the compressor unstable), the transient slope can be negative (and thus the compressor stable) if the transient time constant is low enough (i.e. if the reduced frequency is high). This has important implications for the inception of rotating stall since the stability of disturbances is dependent on the effective slope of the pressure rise characteristic. Specifically, inclusion of the time lag can increase compressor stability.

COMPRESSOR STABILITY MODELING

The analytical model used in this study is an extension to the one described in Moore (1984), Hynes and Greitzer (1987), and Epstein, Ffowcs Williams, and Greitzer (1989). The analysis is two-dimensional, which is appropriate since the machine under consideration has a high hub-to-tip ratio. The inlet flow field is undistorted (uniform inlet total pressure), and the inlet and exit ducts are assumed long, so that end effects, i.e. reflection and scattering of the disturbance wave from the ends, are not important. In addition, the tip speed of the compressor is assumed to be low enough for the flow field to be considered incompressible.

In the analysis an arbitrary flow perturbation, $\delta\phi$ is assumed to be of the form:

$$\delta\phi = \sum_{n=1}^{\infty} A_n e^{s_n \bar{t}} e^{in\vartheta}, \tag{5}$$

where

$$s_n = \frac{(\alpha_n - i\omega_n)r}{U}. \tag{6}$$

The rotation rate of the n'th spatial harmonic non-dimensionalized by the rotor rotational speed is represented by $\omega_n r/nU$, while $\alpha_n r/U$ represents the non-dimensionalized growth rate of the n'th spatial harmonic. When the above form of the flow coefficient perturbation is substituted into the differential equations describing the dynamics of the fluid in the compression system, the analysis yields an eigenvalue problem in s_n, with the growth and rotation rates of each spatial harmonic determined from the solution to the eigenvalue problem. If the real part of s_n is negative, the spatial harmonic is damped, and the compressor operation is stable; if the real part of s_n is positive, the spatial harmonic grows exponentially, so that the compressor is unstable. Details of the extension of the stability modeling to account for finite compressor response time can be found in Appendix A.

The analysis must then be extended to include the effects of active feedback control. Control is implemented by the temporal and spatial variation of the control vane stagger angles in response to a measured inlet axial velocity distribution. The spatial variation in the control vane stagger angle has two effects on the compressor inlet flow. The first is an inlet flow angle variation to the first rotor with an associated variation in pressure rise. The second is a variation in flow blockage in the compressor which is a consequence of the variation in blade passage geometry around the annulus of the compressor. Paduano et al. (1991) developed a semi-actuator disk model of the control vanes which accounts for both of these effects. In the present study, this vane model is retained, but the compressor model is extended to account for the finite response time of the compressor pressure rise to both axial velocity fluctuations and control vane deflections. The modeling of the actuation system includes the time delay between velocity sensing and the controller command to the guide vane servo-motors, and the dynamic response of the control vane/ servo-motor assembly to the controller command. To illustrate the analysis technique, a derivation of the model with a simplified version of the controller and actuator dynamics is given in Appendix B.

SYSTEM IDENTIFICATION OF COMPRESSOR DYNAMICS

Paduano showed that the response of compressor flow perturbations to control vane deflections can be expressed in transfer function form as,

$$\frac{\delta\phi_1}{\delta\gamma} = \frac{(iG_n s + A_n + iB_n)(a_{n1} + a_{n2}s + a_{n3}s^2 + \ldots + a_{nj}s^j)}{(s - C_n - iD_n)(b_{n1} + b_{n2}s + b_{n3}s^2 + \ldots + b_{nk}s^k)} \tag{7}$$

where s represents the complex frequency (growth rate and rotation speed) of the forcing function; $\delta\gamma$, the control vane deflection wave; and ϕ_1 refers to the flow coefficient at the measurement station. The transfer function developed from the compression system model in Appendix B can be written in an equivalent form, hence the model parameters can be related directly to those determined experimentally. In particular, C_n corresponds to the growth rate α_n, and D_n to the rotation rate ω_n of the n'th spatial harmonic. $(-B_n/G_n)$ and (A_n/G_n) represent the growth rate and frequency of the forced perturbation wave at which the actuation system is ineffective at producing a flow perturbation response. (This is defined as a *zero* of the actuation system.) In addition, G_n represents the effectiveness of the compression system to control vane forcing over the frequency range. The parameters A_n, B_n, C_n, D_n, and G_n therefore completely specify the open loop behavior of the compressor/actuation system. The parameters in Eq. (7) were experimentally determined using a least squares algorithm to fit the form of the transfer function to the measured dynamic response of the compressor. The accuracy of the theoretical model as a quantitative predictive tool could therefore be established by comparing the experimentally determined parameters to those predicted theoretically.

Open Loop Identification Methodology

In the development of the hydrodynamic stability model, it is assumed that the spatial harmonics of disturbance waves are decoupled, so that a linear model could be used. This assumption should be valid for the experimental identification studies so long as both the forcing and response disturbances are small in amplitude. Since the compressor characteristic slope plays an important role in the dynamics, a unique transfer function exists at each steady-state operating point for each spatial harmonic of the disturbance wave. In the experiment, the forced response was determined with the compressor operating in both the stable and normally unstable range. In the normally unstable operating range, the compressor was operated under closed loop active control. Under active control, it is the dynamic response of the combination of the compressor and the control system that is measured, therefore it is necessary to also accurately characterize the dynamics of the control system, so that compressor transfer can be deduced from measurements of the overall system.

The basic approach is to excite the compressor with a well-characterized disturbance (a small amplitude sine wave deflection of the control vanes travelling about the circumferences at various speeds is a simple example). To generate the data presented herein, on the normally stable portion of the compressor map, a pseudo-random binary excitation signal with a bandwidth 1.25 times the rotor's rotational frequency was used to excite the dynamics of the first three spatial harmonics. Identification studies of harmonics higher than three would have

TABLE 2
PARAMETER IDENTIFICATION DATA

				1st Harmonic				
ϕ	Percent Difference from ϕ_{stall}	$C_1 = \alpha_1$	$D_1 = \omega_1$	A_1	B_1	G_1	Re(zero)= $-B_1 / G_1$	Im(zero)= A_1 / G_1
0.488	6.0	-0.1839	0.329	-0.0709	0.00280	-0.0573	0.0489	1.238
0.462	0.4	-0.0303	0.304	-0.0650	0.00375	-0.0515	0.0728	1.262
0.432	-6.0	0.1320	0.270	-0.0463	0.00943	-0.0329	0.2865	1.406
				2nd Harmonic				
ϕ	Percent Difference from ϕ_{stall}	$C_2 = \alpha_2$	$D_2 = \omega_2$	A_2	B_2	G_2	Re(zero)= $-B_2 / G_2$	Im(zero)= A_2 / G_2
0.488	6.0	-0.2829	0.790	-0.1119	-0.01525	-0.0872	-0.1749	1.283
0.460	0.0	-0.1223	0.762	-0.1032	-0.00446	-0.0724	-0.0616	1.426
0.432	-6.0	0.0510	0.781	-0.0684	0.00345	-0.0431	0.0799	1.587

required control vane forcing at a frequency beyond the bandwidth of the actuation system. The transfer function was then determined from simultaneous discrete-time measurements of the control vane deflections, and flow field velocity perturbations around the compressor annulus, using a spectral method. The transfer function of each spatial harmonic resembled a second order dynamic system, which is equivalent to a first order system with complex coefficients of the form,

$$\frac{\delta\phi_1}{\delta\gamma} = \frac{iG_n s + A_n + iB_n}{s - C_n - iD_n} \tag{8}$$

which indicates that the additional terms in Eq. (7) do not affect the transfer function significantly. From the order of magnitude of the coefficients of the additional terms in the theoretical model, one can deduce that they will not affect the shape of the transfer function significantly over the range of forcing frequencies that was used in the experiment. Figures 17 and 18 show a least squares fit of the transfer function of the form in Eq. (8) to the experimental data. The fidelity of fit indicates that the form of Eq. (8) is quite appropriate for this compressor. The fit parameters which therefore form the dynamic model of this compressor are given in Table 2.

When the spatial harmonic of interest was stabilized by closed-loop control, the transfer function could not be determined directly in the above manner. In this case, the parameters describing the open-loop performance were calculated using an instrument-variable modeling technique adapted to compressor identification by Paduano (1991). This method required an accurate model of the actuator dynamics, and a quantitative

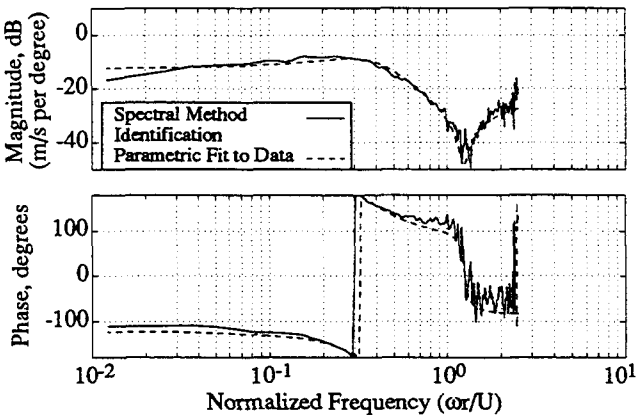

Fig. 17: Estimate of compressor transfer function for first harmonic at ϕ = 0.49 (6% above the stalling flow coefficient.

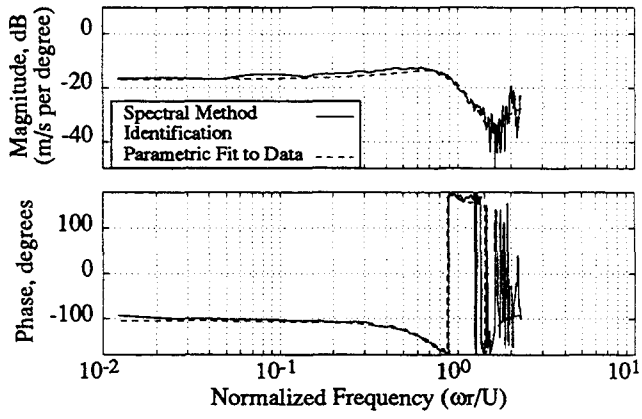

Fig. 18: Estimate of compressor transfer function for second harmonic at ϕ = 0.49 (6% above the stalling flow coefficient.

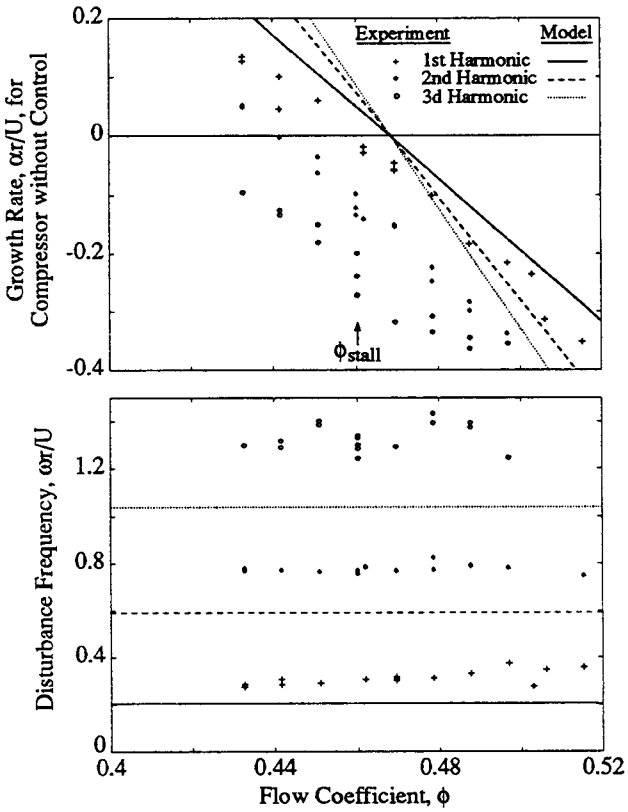

Fig. 19: Measured wave growth and rotational rates compared with predictions of the unmodified Moore-Greitzer model for the first three spatial harmonics.

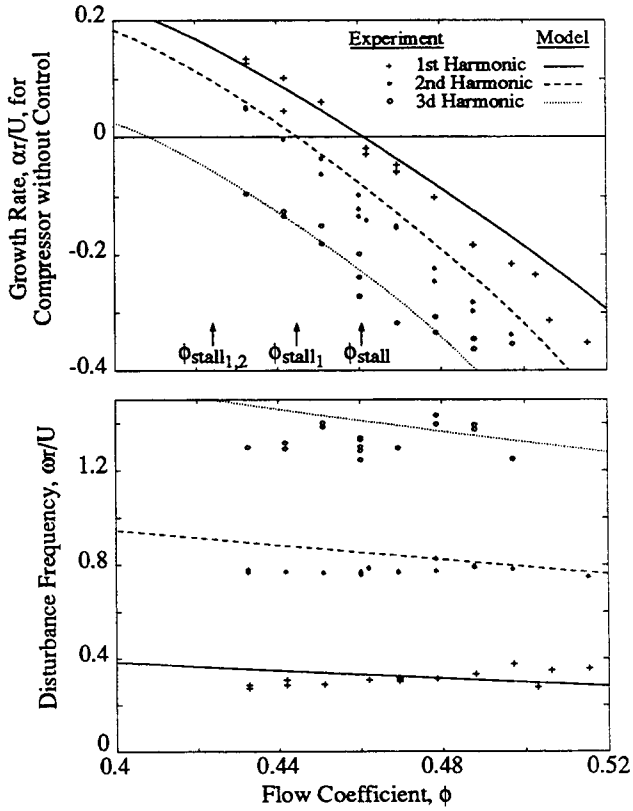

Fig. 20: Measured wave growth and rotational rates compared with predictions of the model modified to account for compressor time lags. The arrows denote the experimentally determined rotating stall initiation points.

estimate of time delays in the feedback system. The actuator dynamics were determined from measurements of the response of control vane motion to the command signal. The open loop transfer function of the compressor was then measured by superimposing a forcing signal on the vane control signal. The accuracy of the instrument-variable method was checked continually by comparing the vane deflections with those simulated by the actuator dynamic model. The open loop dynamic parameters of the compressor could then be obtained from the commanded forcing perturbation, the actual vane deflections, and measurements of velocity perturbations upstream of the compressor. The details of the procedure are described by Haynes (1992).

COMPARING OPEN LOOP MEASUREMENTS AND PREDICTIONS

The symbols in Fig. 19 show the growth rates and frequencies of the first three spatial harmonics of a disturbance wave determined from the experimental identification studies. Negative values of $\alpha_n r/U$ represent temporal decay of a spatial harmonic while positive values represent exponentially growth. The experimental data shows that the spatial harmonics of the disturbance wave become unstable sequentially as ϕ is decreased, with higher harmonics becoming unstable at lower flow coefficients. The spacing of the neutral stability points ($\alpha_n = 0$) of the spatial harmonics is important for active control of rotating stall in compressors, since it gives an indication of the range extension that could be achieved for each additional spatial harmonic that is controlled.

With no control, the identification data indicates that rotating stall would be triggered by the growth of the first spatial harmonic where $\alpha_1 = 0$ at a flow coefficient of $\phi = 0.46$. The time history of spatial harmonic coefficients shown in Fig. 9 does indeed show that a coherent first harmonic perturbation appears first here and grows in amplitude before the higher harmonics do.

Figure 19 shows the prediction of the unmodified Moore-Greitzer model (which does not include the effects of finite compressor time response) that all the spatial harmonics of the disturbance wave become unstable at the same flow coefficient, $\phi = 0.468$, which is the peak of the total-to-static pressure rise characteristic. Also, the model underpredicts the rotational frequencies of the spatial harmonics. The model modified to include finite response times, however, gives much better agreement with the experimental data (Fig. 20). Since the exact values of the compressor blade row time lags needed by the model were not known *a priori*, a parametric study was done to

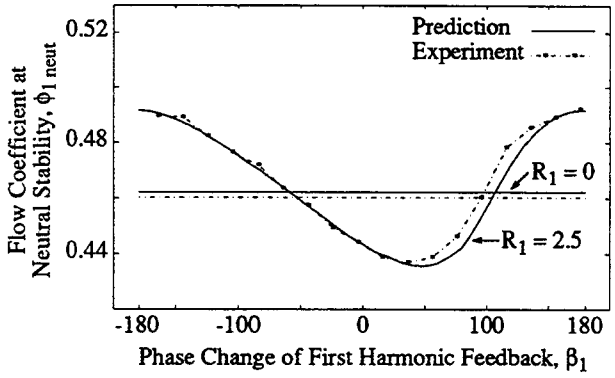

Fig. 21: The influence of the first spatial harmonic controller phase angle, β_1, on stalling flow coefficient at two controller gains, R.

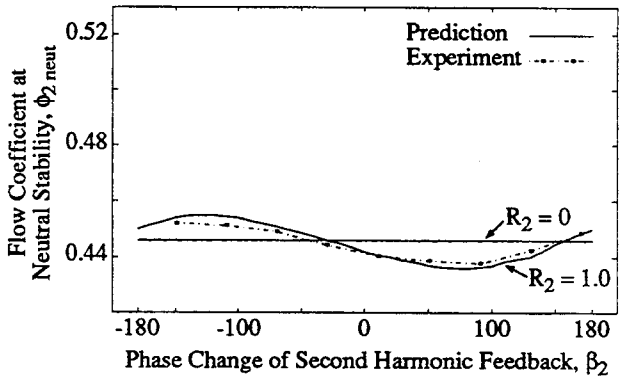

Fig. 22: The influence of the second spatial harmonic controller phase angle, β_2, on stalling flow coefficient at two controller gains, R.

determine the effect of their variation on the resultant theoretical predictions. In Fig. 20, the blade row response times $\bar{\tau}_s$ and $\bar{\tau}_r$ are set equal to 1.5 times the blade passage convection times, which gave the best agreement of the model with the experimental data. It is important to note that the growth and rotation rates of all three harmonic disturbances (6 quantities in total) predicted by the model show good agreement with data when only one constant is adjusted, the blade row time lag. Furthermore, the value required to match the data, 1.5 times the blade passage convection time, is within the range found by Nagano et al. (1971) whose experiments to characterize the response time produced values of between 1 and 1.5. This supports the hypothesis that finite pressure rise response time is the physical mechanism causing the sequential destablizing of the spatial harmonics of the flow coefficient perturbation.

PREDICTING CLOSED LOOP COMPRESSOR BEHAVIOR

As was discussed above, the modified compressor stability model does a good job of predicting the open loop dynamics of the system, implying that the compressor dynamics are appropriately represented. This model adapted to the closed loop system should then be able to predict both the behavior of the compressor under active control as well as the influence of control system design parameters on that behavior. Details of the closed loop model are given in Appendix B.

Figure 21 shows the boundary between stable and unstable operation of the compressor operating under closed loop active control of the first spatial harmonic, as the phase of the control vane deflection wave is varied relative to that of the measured velocity perturbation wave. The flow coefficient at which the spatial harmonic becomes unstable with no feedback control (gain, R = 0) is also shown. The operating range of the compressor is thus extended for those phases for which the closed loop stability boundary is lower than the uncontrolled neutrally stable flow coefficient. The control system has a destabilizing effect on the compressor where the stability boundary is greater. The optimum feedback phase is that which gives the largest range extension and corresponds to the trough of the closed loop stability curve.

The model prediction and the experimental results in Fig. 21 agree closely. The agreement for control of the second spatial harmonic is close as well (Fig. 22), suggesting that the model is indeed an accurate representation of the stabilized compressor dynamics.

DISCUSSION AND SUMMARY

We have presented herein details of the closed loop control of a three-stage low speed research compressor. In addition to being only an end unto itself, the actively stabilized compressor is a powerful research tool for use in the understanding of compressor dynamics. In particular, such a machine facilitates the accurate measurement of the compression system dynamics with a combination of forced response experiments and system identification methodology. We have found the adoption of controls formalization to be a great aid in this area of fluid mechanics research.

Two approaches were taken to establish the compressor dynamics: (1) experimental measurement and identification, and (2) an analytical hydrodynamic 2-D stability model of the flow field. The experimental data was used to determine the relative importance of fluid phenomena included in the modeling. In this case, compressor time lags due to losses proved to be important while those stemming from deviation and blockage were not. The Moore-Greitzer stability model when suitably modified to include these time lags accurately predicted the open loop onset of stall as well as the behavior of the stabilized compressor. This implies that, to the degree to which these results may now be generalized, a tool now exists for predicting the rotating stall point in high hub-to-tip ratio compressors for which compressibility is not important.

What limits the improvement in compressor operating range achievable with active stabilization, and are these limits predicted by theory? As the compressor operating point is moved to lower mass flows and the characteristic slope increases, the controller gain must be increased. At some point, however, the bandwidth and control authority of the stabilization system will be inadequate to maintain stability. The drop-off of control authority with frequency is exacerbated with variable angle control vane

actuators because of unfavorable dynamic behavior. The vanes change the flow angle into the rotor (the primary control mechanism) but also the convergent/divergent passages formed between the vanes (depending on stagger angle distribution) simultaneously introduce an additional circumferential flow variation which influences the compressor stability. These two effects have differing frequency response and sign, so as the vane frequency is increased, they can cancel each other, reducing the net control authority. When the control loop is closed by sensing axial velocity upstream of the control vanes (as is the case here), a non-minimum phase zero is introduced limiting controller effectiveness. (Calculations indicated that moving the sensors downstream of the control vanes can alleviate this problem by altering the system phase lags and thereby increase the stable compressor operating range. This has yet to be verified experimentally, however.)

The limits imposed by actuator effectiveness and sensor placement notwithstanding, the theory predicts that the controller gain (R) could be increased by a factor of two over the values used in this work with a concomitant increase in stable operating range. Experimentally, however, the higher controller gain yielded no improvement in performance. Why? At the higher gain, the model indicates that there is very little margin for error in the setting of the feedback parameters, while we know that, at the very least, there is uncertainty in such parameters as the characteristic slope ($\partial\psi/\partial\phi$) and control authority ($\partial\psi/\partial\gamma$), whether derived from aerodynamic theory or parametric fits. In addition, considerable noise (uncharacterized unsteadiness) is present on all measurements in a multi-stage compressor. Thus, we attribute the difference between the theoretical and empirical gain limits to modeling uncertainty (a sophisticated way of saying that we are not certain of the cause). Control theorists have developed a considerable body of knowledge concerning the design of controllers for systems with parametric uncertainty, but we have yet to apply it in this case.

Since control of the first two harmonics confirms quite closely to theory at the lower gains, Hendricks and Gysling (1992) have used this modeling approach to examine the performance of alternate actuators in controlling this compressor. They predicted that a circumferential array of jets at the compressor inlet in place of the control vanes should be particularly effective, stabilizing the compressor down to a characteristic slope of 4, over four times that achievable with control vanes, with a concomitant increase in stable flow range. Work is proceeding on an experimental verification of this analysis.

Overall, we believe that the good agreement between the experiment and theory presented herein indicates that it is now possible to assess analytically the influence of active compressor stabilization on the dynamics of the type of machine tested. Work is ongoing to extend the modeling and experiment to include low hub-to-tip ratio compressors (a 3-D stability model), to account for the effects of compressibility, and to treat the influence of inlet distortion on actively stabilized compressors.

ACKNOWLEDGEMENTS

The authors wish to thank Professors J.D. Paduano and E.M. Greitzer for much help and thoughtful discussion. This work was supported by the Air Force Office of Scientific Research, Major D. Fant, technical monitor.

REFERENCES

Day, I.J., "Active Suppression of Stall and Surge in Axial Compressors," Proceedings, ASME/IGTI Conference in Orlando, FL, 1991.

Emmons, H.W, Pearson, C.E., and Grant, H.P., "Compressor Surge and Stall Propagation", *ASME Transactions*, Vol. 79, pp.455-469, 1955.

Epstein, A.H., Ffowcs Williams, J.E., Greizer, E.M., "Active Suppression of Aerodynamic Instabilities in Turbomachines", *Journal of Propulsion and Power*, V.5, No 2, 1989, pp. 204-211.

Etchevers, O., "Evaluation of Rotating Stall Warning Schemes for Axial Compressors," M.S. Thesis, Department of Aeronautics and Astronautics, MIT, 1992.

Ffowcs Williams, F.E., Huang, X., "Active Stabilization of Compressor Surge," *Journal of Fluid Mechanics*, Vol. 204, 1989, pp. 245-262.

Gamache, R.N., "Axial Compressor Reversed Flow Performance," Ph.D. Thesis, Department of Aeronautics and Astronautics, MIT, 1985.

Garnier, V.H., Epstein, A.H., Greitzer, E.M., "Rotating Waves as a Stall Inception Indication in Axial Compressors", *Journal of Turbomachinery*, Vol. 113, 1991, pp. 290-301.

Haynes, J., "Active Control of Rotating Stall in a Three-Stage Axial Compressor," M.S. Thesis, Department of Mechanical Engineering, MIT, 1992.

Hendricks, G.J., and Gysling, D.L., "A Theoretical Study of Sensor-Actuator Schemes for Rotating Stall Control", presented at the AIAA/SAE/ASME/ASEE 28th Joint Propulsion Conference and Exhibit, Nashville, TN, 1992.

Hynes, T.P., and Greitzer, E.M., "A Method for Assessing Effects of Circumferential Flow Distortion on Compressor Stability", *Journal of Turbomachinery*, Vol. 109, pp. 371-379, 1987.

Lavrich, P.L., "Time Resolved Measurements of Rotating Stall in Axial Flow Compressors," MIT GTL Report No. 194, 1988.

Longley, J.P., Hynes, T.P., "Stability of Flow Through Multistage Axial Compressors," ASME Paper 89-GT-311, 1989.

Mazzawy, R.S., "Multiple Segment Parallel Compressor Model for Circumferential Flow Distortion", *Journal of Engineering for Power*, Vol. 99, No. 2, 1977.

McDougal, N.M, Cumpsty, N.A., Hynes, T.P., "Stall Inception in Axial Compressors", *Journal of Turbomachinery*, Vol. 112, 1990, pp. 116-125.

Moore, F.K., "A Theory of Rotating Stall of Multistage Axial Compressors: Part I - Small Disturbances", *Journal of Engineering for Gas Turbines and Power*, Vol. 106, 1984, pp. 313-320.

Moore, F.K., Greitzer, E.M., "A Theory of Post-Stall Transients in Axial Compressors: Part I - Development of the Equations," *ASME Journal of Engineering for Gas Turbines and Power*, Vol. 108, 1986, pp. 68-76.

Nagano, S., Machida, Y., Takata, H, "Dynamic Performance of Stalled Blade Rows", Japan Society of Mechanical Engineering Paper JSME 11, Presented at the Tokyo Joint International Gas Turbine Conference, Tokyo, Japan, 1971.

Paduano, J. D., "Active Control of Rotating Stall in Axial Compressors", Ph.D Thesis, Department of Aeronautics and Astronautics, MIT, 1991.

Paduano, J., Epstein, A.H., Valavani, L., Longley, J.P., Greitzer, E.M., Guenette, G.R., "Active Control of Rotating Stall in a Low Speed Axial Compressor", ASME paper 91-GT-88, Presented at the International Gas Turbine and Aeroengine Congress and Exposition, Orlando, FL, 1991.

Pinsley, J.E., Guenette, G.R., Epstein, A.H., Greitzer, E.M., "Active Stabilization of Centrifugal Compressor Surge," *ASME Journal of Turbomachinery*, Vol. 113, 1991.

APPENDIX A
COMPRESSOR STABILITY MODEL INCLUDING TRANSIENT BEHAVIOR

In this model, the pressure rise across a compressor is modified by the pressure difference required to overcome the inertia of the fluid within the blade channels when the flow within the compressor is unsteady. If one assumes that the flow within the blade passages is one dimensional, the unsteady pressure rise across the compressor can be written as (Moore, 1984; Hynes and Greitzer, 1987):

$$\frac{P_e - P_{ti}}{\rho U^2} = \psi - \lambda \frac{\partial \phi}{\delta \vartheta} - \frac{\mu r}{U} \frac{\partial \phi}{\partial t} \tag{A1}$$

where:

$$\psi = \psi_{isen} - L_r - L_s \tag{A2}$$

ψ_{isen} is the isentropic stagnation pressure rise across the compressor and L_r and L_s are the rotor and stator stagnation pressure losses. The inertia of the fluid in the rotors and in the compressor are represented by λ and μ respectively. At the inception of rotating stall, the flow coefficient through the compressor is modified by a small perturbation $\delta\phi$ so that:

$$\phi = \bar{\phi} + \delta\phi \qquad \psi_{isen} = \bar{\psi}_{isen} + \frac{d\bar{\psi}_{isen}}{d\phi}\delta\phi$$

$$P_e = \bar{P}_e + \delta P_e \qquad L_s = \bar{L}_s + \delta L_s \tag{A3}$$

$$P_{ti} = \bar{P}_{ti} + \delta P_{ti} \qquad L_r = \bar{L}_r + \delta L_r$$

The compressor pressure rise perturbation equation is therefore:

$$\frac{\delta P_e - \delta P_{ti}}{\rho U^2} = \frac{d\bar{\psi}_{isen}}{d\phi}\delta\phi - \delta L_s - \delta L_r - \lambda \frac{\partial(\delta\phi)}{\partial \vartheta} - \frac{\mu r}{U}\frac{\partial(\delta\phi)}{\partial t} \tag{A4}$$

$$\bar{\psi}_{isen} = \bar{\psi} + \bar{L}_r + \bar{L}_s \tag{A5}$$

where $\bar{\psi}$ is the steady, axisymmetric total-to-static pressure rise including losses, and $\bar{L}_s$ and $\bar{L}_r$ the steady stator and rotor stagnation pressure losses respectively. The stator transient stagnation pressure loss perturbation, δL_s, is given by the differential equation:

$$\tau_s \frac{\partial(\delta L_s)}{\partial t} = \frac{\partial \bar{L}_s}{\partial \phi}\delta\phi - \delta L_s \tag{A6}$$

The rotor transient stagnation pressure loss, δL_r, is calculated in a reference frame rotating with the rotor:

$$\tau_r \left(\frac{\partial(\delta L_r)}{\partial t} + \frac{U}{r}\frac{\partial(\delta L_r)}{\partial \vartheta} \right) = \frac{\partial \bar{L}_r}{\partial \phi}\delta\phi - \delta L_r \tag{A7}$$

In this analysis, a general perturbation in flow coefficient of the form:

$$\delta\phi = \sum_{n=1}^{\infty} A_n e^{(\alpha_n - i\omega_n)t} e^{in\vartheta} \tag{A8}$$

is considered. Each spatial harmonic of the perturbation can be considered separately, so only the *n'th* spatial harmonic:

$$\delta\phi_n = A_n e^{(\alpha_n - i\omega_n)t} e^{in\vartheta} \tag{A9}$$

will therefore be examined.

The variables describing the evolution of the perturbation can be non-dimensionalized as follows:

$$\bar{t} = \frac{tU}{r}, \qquad \bar{\tau} = \frac{\tau U}{r}, \qquad s_n = \frac{(\alpha_n - i\omega_n)r}{U}, \tag{A10}$$

where U is the rotor speed and r is the average radius of the compressor annulus, so that the equations describing the perturbation become:

$$\frac{\delta P_e - \delta P_{ti}}{\rho U^2} = \frac{d\psi_{isen}}{d\phi}\delta\phi_n - \delta L_s - \delta L_r - \lambda \frac{\partial(\delta\phi)}{\partial \vartheta} - \mu \frac{\partial(\delta\phi)}{\partial \bar{t}} \tag{A11}$$

$$\bar{\tau}_s \frac{\partial(\delta L_s)}{\partial \bar{t}} = \frac{\partial \bar{L}_s}{\partial \phi}\delta\phi_n - \delta L_s \tag{A12}$$

$$\bar{\tau}_r \left(\frac{\partial(\delta L_r)}{\partial \bar{t}} + \frac{\partial(\delta L_r)}{\partial \vartheta} \right) = \frac{\partial \bar{L}_r}{\partial \phi}\delta\phi_n - \delta L_r \tag{A13}$$

$$\delta\phi_n = A_n e^{s_n \bar{t}} e^{in\vartheta} \tag{A14}$$

The upstream stagnation and downstream static pressure

perturbations are given by the expressions (Epstein, Ffowcs Williams, Greitzer, 1989):

$$\frac{\delta P_{ti}}{\rho U^2} = -\frac{1}{|n|}\frac{\partial(\delta\phi_n)}{\partial\bar{t}}, \tag{A15}$$

and

$$\frac{\delta P_e}{\rho U^2} = \frac{1}{|n|}\frac{\partial(\delta\phi_n)}{\partial\bar{t}} \tag{A16}$$

Substitution of Eqs. (A15), (A16) and (A14) into Eqs. (A11)-(A13) produces a generalized, complex eigenvalue problem in s_n:

$$(A - s_n B)\,\delta\bar{x} = 0 \tag{A17}$$

where:

$$A = \begin{pmatrix} \frac{1}{\zeta}\left(\frac{d\bar{\psi}_{isen}}{d\phi} - in\lambda\right) & -\frac{1}{\zeta} & -\frac{1}{\zeta} \\ \frac{1}{\bar{\tau}_s}\frac{d\bar{L}_s}{d\phi} & -\frac{1}{\bar{\tau}_s} & 0 \\ \frac{1}{\bar{\tau}_r}\frac{d\bar{L}_r}{d\phi} & 0 & -\left(in + \frac{1}{\bar{\tau}_r}\right) \end{pmatrix} \tag{A18}$$

$$B = \begin{pmatrix} 1 & 0 & 0 \\ 0 & 1 & 0 \\ 0 & 0 & 1 \end{pmatrix} \tag{A19}$$

$$\delta\bar{x} = \begin{pmatrix} \delta\phi_n \\ \delta L_s \\ \delta L_r \end{pmatrix} \tag{A20}$$

$$\zeta = \left(\frac{2}{|n|} + \mu\right) \tag{A21}$$

and

$$\bar{\psi}_{isen} = \bar{\psi} + \bar{L}_r + \bar{L}_s . \tag{A22}$$

The solution to the eigenvalue problem yields the growth and rotation rates of the perturbation wave. If the real part of s_n is negative, the disturbance is damped, representing stable operation of the compressor. If the real part of s_n is positive, the disturbance grows exponentially, representing unstable operation. For the uncontrolled compressor the growth rate of the perturbation is determined by the slope of the total-to-static pressure rise characteristic.

We must now fit this model to our data. The steady state compressor slope, $d\bar{\psi}/d\phi$ is determined from a polynomial fit to the measured pressure rise data. The total pressure loss across the compressor is estimated from the difference between the isentropic pressure rise characteristic and the measured one. A polynomial fit to this estimate is then used to determine the slopes of the rotor and stator loss curves, $d\bar{L}_r/d\phi$ and $d\bar{L}_s/d\phi$. For the particular build of the three stage compressor that was considered (75% reaction), it was assumed that 75% of the steady total pressure losses occurred across the rotors, and 25% across the stators. The time constants $\bar{\tau}_s$ and $\bar{\tau}_r$ were related to the convection time of the bulk flow through the blade channels. Since the values of these constants were not measured, a parametric study was done by varying these constants about the blade passage convection time. The best agreement with the experimental data was obtained with the time constants set to 1.5 times the blade passage convection time.

APPENDIX B
COMPRESSOR STABILITY MODEL INCLUDING ACTIVE CONTROL

In an actively controlled compressor, the relation between pressure and velocity perturbations can be manipulated by the actuator. Analysis of the movable inlet guide vane actuator involves determining relations between the actuation and perturbations in velocity and pressure introduced into the flow field. The actuator is modeled using quasi-steady actuator disk theory. A detailed model of the compressor with control vane control is given by Paduano (1991) and Paduano et al. (1991), and is outlined here, with modifications to account for finite compressor response times. With control vanes and quasi-steady compressor response the compressor perturbation equation for each spatial harmonic can be written as:

$$\frac{\delta P_e - \delta P_{t2}}{\rho U^2} = \frac{\partial\psi}{\partial\phi}\delta\phi_2 + \frac{\partial\psi}{\partial\gamma}\delta\gamma - \lambda\frac{\partial(\delta\phi_2)}{\partial\vartheta} - \mu\frac{\partial(\delta\phi_2)}{\partial\bar{t}} \tag{B1}$$

where,

$$\frac{\delta P_e}{\rho U^2} = \frac{1}{|n|}\frac{\partial(\delta\phi_2)}{\partial\bar{t}} \tag{B2}$$

and

$$\frac{\delta P_{t2}}{\rho U^2} = \frac{\delta P_{t1}}{\rho U^2} - \mu_{igv}\frac{\partial}{\partial\bar{t}}\left(\delta\phi_2 + \frac{1}{2}\phi\mu_{igv}\frac{\partial(\delta\gamma)}{\partial\vartheta}\right) \tag{B3}$$

with

$$\delta\phi_2 = \delta\phi_1 - in\phi\mu_{igv}\delta\gamma \tag{B4}$$

and

$$\frac{\delta P_{t1}}{\rho U^2} = -\frac{1}{|n|}\frac{\partial(\delta\phi_1)}{\partial\bar{t}} \tag{B5}$$

Here $\delta\gamma$ represents an angular displacement of the inlet guide vanes from their mean position. When the quasi-steady assumption is relaxed, and the finite compressor response times are modeled, the compressor perturbation equation can be written as:

$$\frac{\delta P_e - \delta P_{t2}}{\rho U^2} = \frac{\partial \overline{\psi}_{isen}}{\partial \phi}\delta\phi_2 + \frac{\partial \overline{\psi}_{isen}}{\partial \gamma}\delta\gamma - \delta L_s$$

$$-\delta L_r - \lambda\frac{\partial(\delta\phi_2)}{\partial \vartheta} - \mu\frac{\partial(\delta\phi_2)}{\partial \bar{t}} \tag{B6}$$

where the transient losses, δL_s and δL_r are now modeled by the following equations,

$$\overline{\tau}_s\frac{\partial(\delta L_s)}{\partial \bar{t}} = \frac{\partial \overline{L}_s}{\partial \phi}\delta\phi_2 - \delta L_s \tag{B7}$$

$$\overline{\tau}_r\left(\frac{\partial(\delta L_r)}{\partial \bar{t}} + \frac{\partial(\delta L_r)}{\partial \vartheta}\right) = \frac{\partial \overline{L}_r}{\partial \phi}\delta\phi_2 + \frac{\partial \overline{L}_r}{\partial \gamma}\delta\gamma - \delta L_r \tag{B8}$$

The above system of equations can be written as a transfer function between the flow perturbation at the measurement location upstream of the IGV's, $\bar{x}_{hw}$, and the control vane deflection $\delta\gamma$,

$$\frac{\delta\phi_{1,hw}}{\delta\gamma} = in\mu_{igv}\phi\, e^{-|n|\bar{x}_{hw}} + \frac{\dfrac{\partial \overline{\psi}_{isen}}{\partial \gamma} - \dfrac{\partial \overline{L}_r/\partial\gamma}{1+\overline{\tau}_r(s+in)} - in\mu_{igv}\phi s\left(\dfrac{1}{|n|}+\dfrac{\mu_{igv}}{2}\right)}{\zeta s + in\lambda - \dfrac{\partial \overline{\psi}_{isen}}{\partial \phi_2} - \dfrac{\partial \overline{L}_s/\partial\phi_2}{1+s\overline{\tau}_s} - \dfrac{\partial \overline{L}_r/\partial\phi_2}{1+\overline{\tau}_r(s+in)}} e^{-|n|\bar{x}_{hw}} \tag{B9}$$

Control is implemented by sensing the axial velocity perturbation, $\delta\phi_1$ upstream of the inlet guide vanes. The measured signal is then processed by the controller which commands the control vanes to introduce a suitable perturbation into the flow field. With the proportional feedback scheme that was employed in the experiment, the measured signal is modified in amplitude and shifted spatially in phase. This is implemented analytically as follows:

$$\delta\gamma|_c = Z\, e^{-|n|\bar{x}_{hw}}\delta\phi_1 \tag{B10}$$

$$Z = Re^{-i\beta n} \tag{B11}$$

where R is the gain in amplitude of the signal, and β_n is the spatial phase shift of the commanded signal relative to the measured signal. In practice, non-ideal behavior causes the output from the actuator to differ from the command given by the controller. The non-ideal actuator dynamics were determined experimentally by measuring the transfer function of the actuator motion relative to an input command signal, and then fitting an appropriate dynamic model to the transfer function. As a simple example, assume that the dynamics of the actuator can be modeled by a second order differential equation,

$$\frac{\partial^2(\delta\gamma)}{\partial \bar{t}^2} + 2\varsigma_a\omega_a\frac{\partial(\delta\gamma)}{\partial \bar{t}} = \omega_a^2\left(\delta\gamma|_c - \delta\gamma\right) \tag{B12}$$

where ω_n and ζ_a are the resonant frequency and damping ratio of the actuation system. (In the experiment a higher order dynamic model was required to accurately match the measured actuator transfer function.) With axial velocity sensing upstream of the control vanes, the actuator equation then becomes:

$$\frac{\partial^2(\delta\gamma)}{\partial \bar{t}^2} + 2\varsigma_a\omega_a\frac{\partial(\delta\gamma)}{\partial \bar{t}} = \omega_a^2\left(Ze^{-|n|\bar{x}_{hw}}\delta\phi_1 - \delta\gamma\right) \tag{B13}$$

Equations (B2)-(B8) and (B10)-(B13) produce an eigenvalue problem. Parameters in the analysis are the operating flow coefficient (which determines the slope of the pressure rise characteristic), the gain and phase of the feedback control law, and the actuator dynamic parameters. For the control vane actuator with velocity feedback, this system of differential equations reduces to the form given in (A17), where the matrices A, B, and the vector $\delta\bar{x}$ are now:

$$A = \begin{pmatrix} \frac{1}{\zeta}\left(\frac{\partial \overline{\psi}_{isen}}{\partial\phi} - in\lambda\right) & -\frac{1}{\zeta} & -\frac{1}{\zeta} & \frac{1}{\zeta}\left(\frac{\partial \overline{\psi}_{isen}}{\partial\gamma}\right) & 0 \\ \frac{1}{\overline{\tau}_s}\frac{\partial \overline{L}_s}{\partial\phi} & -\frac{1}{\overline{\tau}_s} & 0 & 0 & 0 \\ \frac{1}{\overline{\tau}_r}\frac{\partial \overline{L}_r}{\partial\phi} & 0 & -\left(in+\frac{1}{\overline{\tau}_r}\right) & \frac{1}{\overline{\tau}_r}\frac{\partial \overline{L}_r}{\partial\gamma} & 0 \\ 0 & 0 & 0 & 0 & 1 \\ Ze^{-|n|\bar{x}_{hw}}\omega_a^2 & 0 & 0 & X & -2\varsigma_a\omega_a \end{pmatrix} \tag{B14}$$

$$B = \begin{pmatrix} 1 & 0 & 0 & 0 & \frac{in\phi\mu_{igv}}{\zeta}\left(\frac{1}{|n|}+\frac{\mu_{igv}}{2}\right) \\ 0 & 1 & 0 & 0 & 0 \\ 0 & 0 & 1 & 0 & 0 \\ 0 & 0 & 0 & 1 & 0 \\ 0 & 0 & 0 & 0 & 1 \end{pmatrix} \tag{B15}$$

$$\delta\bar{x} = \begin{pmatrix} \delta\phi_2 \\ \delta L_s \\ \delta L_r \\ \delta\gamma \\ \partial(\delta\gamma)/\partial\bar{t} \end{pmatrix} \tag{B16}$$

with:

$$\zeta = \left(\frac{2}{|n|}+\mu\right) \tag{B17}$$

$$\overline{\psi}_{isen} = \overline{\psi} + \overline{L}_r + \overline{L}_s \tag{B18}$$

and

$$X = \omega_a^2(Ze^{-|n|\bar{x}_{hw}}in\phi\mu_{igv} - 1) \tag{B19}$$

There are five eigenvalues for each spatial harmonic of the disturbance, and the system is stable when the real part of each of the eigenvalues is negative.